



Article

Surface Engineering of Carbon-Based Microelectrodes for High-Performance Microsupercapacitors

Liang He ^{1,*}, Tianjiao Hong ¹, Yue Huang ¹, Biao Xiong ¹, Xufeng Hong ¹, Muhammad Tahir ¹, Waqas Ali Haider ¹ and Yulai Han ^{2,*}

¹ State Key Laboratory of Advanced Technology for Materials Synthesis and Processing, Wuhan University of Technology, Wuhan 430070, China; hongtj@whut.edu.cn (T.H.); hyhuangyuehy@gmail.com (Y.H.); nanobear@whut.edu.cn (B.X.); 1316824174@whut.edu.cn (X.H.); tahir@whut.edu.cn (M.T.); haider@whut.edu.cn (W.A.H.)

² School of New Materials and New Energies, Shenzhen Technology University, Shenzhen 518118, China

* Correspondence: hel@whut.edu.cn (L.H.); hanyulai@sztu.edu.cn (Y.H.)

Received: 14 April 2019; Accepted: 29 April 2019; Published: 7 May 2019



Abstract: In this research, the enhancement in electrochemical performance of pyrolyzed carbon microelectrodes by surface modification is investigated. For the proposed microfabrication process, pyrolyzed carbon microelectrodes with multi-walled carbon nanotubes (MWCNTs) on their surface are obtained by developing GM-1060 photoresist in mixture of propylene glycol methyl ether acetate (PGMEA) and CNTs, and following pyrolysis of a micropatterned photoresist. Polyvinyl alcohol (PVA)/H₂SO₄ electrolyte (1 M) was applied to assemble this carbon/CNT microelectrode-based all-solid-state microsupercapacitor (carbon/CNT-MS). The carbon/CNT-MS shows a higher electrochemical performance compared with that of pyrolyzed carbon microelectrode-based MS (carbon-MS). The specific areal and volumetric capacitances of carbon/CNT-MS (4.80 mF/cm² and 32.0 F/cm³) are higher than those of carbon-MS (3.52 mF/cm² and 23.4 F/cm³) at the scan rate of 10 mV/s. In addition, higher energy density and power density of carbon/CNT-MS (2.85 mWh/cm³ and 1.98 W/cm³) than those of carbon-MS (2.08 mWh/cm³ and 1.41 W/cm³) were also achieved. This facile surface modification and optimization are potentially promising, being highly compatible with modern microfabrication technologies and allowing integration of highly electrically conductive CNTs into pyrolyzed carbon to assemble MSs with improved electrochemical performance. Moreover, this method can be potentially applied to other high-performance micro/nanostructures and microdevices/systems.

Keywords: microelectrode; supercapacitor; carbon

1. Introduction

Supercapacitors (SCs), an important kind of energy storage device, have many advantages over traditional energy storage devices [1–3]. There are three kinds of SCs employed in energy storage, namely electrical double layer capacitors (EDLCs), pseudocapacitors, and hybrid SCs. Among these three kinds of SCs, EDLCs are the most commonly applied and studied SCs due to their high stability and low cost. For EDLCs, the charge is stored electrostatically in the Helmholtz layer at the interface of the electrode and electrolyte. EDLC electrodes usually have high specific surface area (SSA) and electrical conductivity such as activated carbons (AC), carbon aerogels, carbon nanotubes (CNTs), graphene, carbide-derived carbon (CDC), and others [4]. Owing to their high SSA and that no chemical reactions occur between electrode and electrolyte, EDLCs usually possess high power density, fast charge/discharge rates, and ultralong lifetimes [5–7].

Microsupercapacitors (MSCs) with interdigital microelectrodes, showing relatively high SSA and short ion diffusion pathways, are of great potential for energy storage microdevices [8,9]. Various fabrication processes for MSCs have been proposed, including photolithography [10–12], inkjet printing [13], laser-irradiation assisted method [14–16], and others. Among these fabrication processes, photolithography is widely used due to its capability of facile control for interdigital microelectrode configuration and full compatibility with current microtechnologies [17–19]. Additionally, micropatterned photoresists can be directly carbonized into porous carbon microstructures which possess good chemical inertness, high reliability, and high electrical conductivity. Furthermore, the pyrolyzed carbon can be employed as a significant component in microdevices/systems such as microcantilevers [20], micromirrors [21], and MSCs [22–28]. In recent years, there are some reported results related to MSCs constructed by pyrolyzed carbon microelectrodes which aim to improve the electrical conductivity, energy storage performance, and cycling stability of pyrolyzed carbon microelectrodes. Yang et al. [26] fabricated an MSC based on photoresist/chitosan-coated carbon nanotube (CHIT-CNT) microelectrode, which has an excellent specific capacitance and high cycling stability over 10,000 cycles. The facile and compatible construction strategy is the critical issue for high-performance MSC.

The microfabrication process of MSC is more important than the choice of electrode materials regarding the reduction of costs. However, previous work has usually focused on how to fabricate the MSC more effectively and ignored the universality of the microfabrication process, and there are a lack of strategies for the optimization of the surface, especially for limited area of MSCs. Surface engineering is an effective way to further improve the performance of a supercapacitor, while rarely applied in MSCs. Herein, developing an advanced surface engineering method for MSCs will expand the optimization strategy to obtain higher electrochemical performance. In this research, a novel surface engineering approach for pyrolyzed carbon microelectrodes is reported. The carbon microelectrodes are derived from a micropatterned GM-1060 negative photoresist (Gersteltec Sarl), which is developed in a mixture of propylene glycol methyl ether acetate (PGMEA) developer and multi-walled carbon nanotubes (MWCNTs), followed by pyrolysis under N_2 flow. By developing the photoresist in a mixture of PGMEA and CNTs, a micropatterned photoresist with CNTs on its surface is obtained. Subsequent pyrolysis of the micropatterned photoresist is conducted under N_2 flow at $900\text{ }^\circ\text{C}$ and 1 M polyvinyl alcohol (PVA)/ H_2SO_4 electrolyte is applied as electrolyte to assemble the all-solid-state MSC. The specific areal capacitance of carbon-MSC is 3.52 mF/cm^2 (23.4 F/cm^3) at the scan rate of 10 mV/s , maximum energy density is 2.08 mWh/cm^3 and maximum power density is 1.41 W/cm^3 . For carbon/CNT-MSC, a higher specific areal capacitance of 4.80 mF/cm^2 (32.0 F/cm^3) was obtained at the scan rate of 10 mV/s , maximum energy density was 2.85 mWh/cm^3 and maximum power density was 1.98 W/cm^3 . By this facile surface modification method, a significant improvement in performance of MSC is achieved. Besides, this method could potentially be used for the application of high-performance microelectrodes.

2. Experimental

2.1. Preparation of the Developer

Fifty milligrams CNTs (purity > 99.9 wt %, XF NANO, Nanjing, China) and 20 mL PGMEA were uniformly mixed together and ultrasonicated for 1 h at room temperature. Afterwards, the mixture was used as the developer for GM-1060 photoresist.

2.2. Microfabrication process of Microsupercapacitor (MSC) with Carbon Nanotubes (CNTs) Modification

Firstly, Si/SiO₂ substrate (3000/500 nm) was rinsed by acetone, isopropanol (IPA), and deionized (DI) water, followed by baking at $135\text{ }^\circ\text{C}$ for 20 min. A uniform GM-1060 negative photoresist layer on the substrate was obtained by spin coating at 2000 rpm for 40 s. The sample was left to cool down to room temperature. After a 5 min, the sample was pre-baked at $65\text{ }^\circ\text{C}$ for 5 min and then $95\text{ }^\circ\text{C}$ for 30 min. Then the sample was exposed to UV light for photolithography. After 5 min, the sample was

post-baked under the same conditions as in the pre-baking process, and was left to cool down to room temperature. Afterwards, the development and rinsing of samples were conducted in PGMEA/CNTs for 3 min and IPA for 30 s, respectively, followed by pyrolysis at 900 °C under N₂ flow for 1 h.

2.3. Characterization and Electrochemical Performance Measurements

Morphology of the fabricated microelectrodes was studied using a field-emission scanning electron microscope (SEM, JEOL JSM-7100F, Tokyo, Japan) at an acceleration voltage of 15 kV. X-ray photoelectron spectroscopy (XPS) measurements were performed using a VG Multilab 2000 instrument for chemical bond characterization. Micro-Raman spectra of the samples were obtained by a Renishaw RM-1000 laser Raman microscope. The electrochemical performances of MSCs were evaluated by a commercial potentiostat (AC Instruments, 660D Model) in 1 M PVA/H₂SO₄ gel polymer electrolyte, which is a mixture of 5 mL H₂SO₄, 10 g PVA, and 100 mL deionized water. The potential window of the cyclic voltammetry tests was 0–0.8 V and the frequency range of electrochemical impedance spectroscopy (EIS) plots was 0.01–100,000 Hz.

3. Results and Discussion

Figure 1a–d demonstrate the microfabrication process of MSC with CNT modification and include three processes: The Si/SiO₂ substrate was cleaned, followed by a baking process. After that, spin coating and photolithography processes were conducted to obtain a uniform interdigital GM-1060 negative photoresist layer on the substrate. Afterwards, the sample was soaked in PGMEA/CNTs for development, followed by annealing treatment to obtain pyrolyzed carbon/CNT microelectrodes.

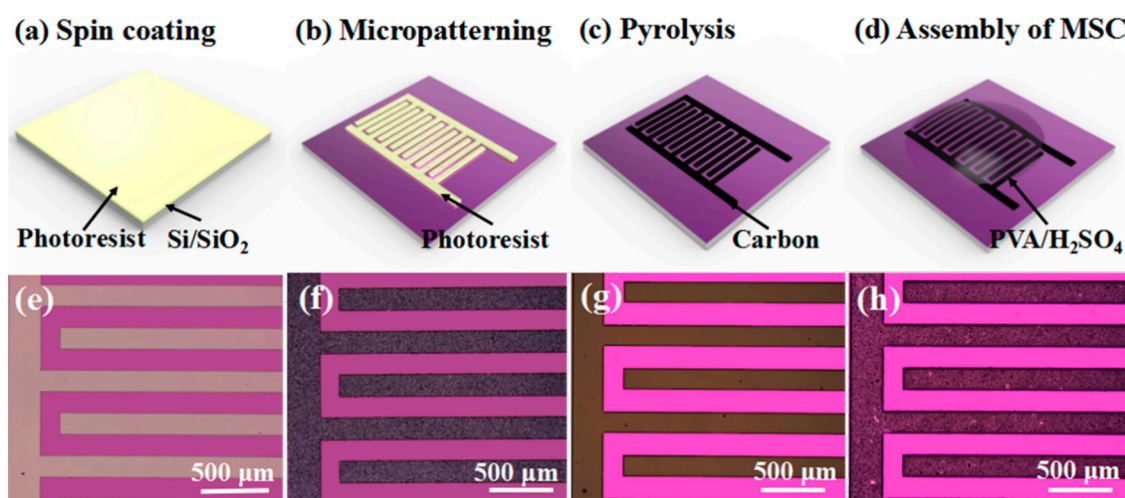


Figure 1. (a–d) Microfabrication process of carbon/CNT microelectrode-based all-solid-state microsupercapacitor (MSC) (carbon/CNT-MSC). (e) Optical image of micropatterned photoresist. (f) Optical image of micropatterned photoresist/CNTs. (g) Optical image of carbon microelectrodes. (h) Optical image of carbon/CNTs microelectrodes.

Figure 1e,g show optical images of the micropatterned photoresist and carbon microelectrodes, respectively. Figure 1f,h show the optical images of the micropatterned photoresist/CNTs and carbon/CNT microelectrodes, respectively. As shown in Figure 1e–h, it is obvious that the micropatterned photoresist and fabricated microelectrodes possess fine and complete micropatterns with no cracks, indicating that this surface modification method is highly suitable for the fabrication of microelectrodes. In addition, the color of the microelectrodes is much darker, and visual differences can be found due to CNT modification. By mixing CNTs with GM-1060 developer, CNTs can be attached to the surface of the photoresist, which will still have a stable attachment with carbon even after pyrolysis, due to the excellent thermal stability of CNTs.

To investigate the state of related elements of GM-1060 before and after pyrolysis, X-ray photoelectron spectroscopy (XPS) was utilized. As shown in Figure 2a, there are main peaks at 284.6 eV for both GM-1060 photoresist and pyrolyzed carbon, indicating the presence of C–C in aromatic rings while a small shoulder at binding energy of ~286.1 eV for GM-1060 photoresist can be seen, implying contribution from different bonding configurations of carbon and oxygen. The intensity of the carbon peak of pyrolyzed carbon is higher than that of the photoresist. It is worth noting that after adsorbing CNTs onto the surface of GM-1060, a weaker C1s peak of that is obtained, due to the polymer coating. As described in Figure 2b,c, the oxygen peak and nitrogen peak of pyrolyzed carbon have disappeared (O1s peaks belong to the adsorbed oxygen in the air), which confirm that the composite of GM-1060 and CNTs has been pyrolyzed completely to carbon. The Raman spectra of pyrolyzed carbon and CNTs are described in Figure 2d to show their microstructure and graphitization degree. As shown in Figure 2d, both a graphitic band (G-band) and disorder-induced band (D-band) are observed. The peak at $\sim 1350\text{ cm}^{-1}$ corresponds to the D-band of the microcrystallite graphite due to enhanced double resonance Raman scattering. Another peak at $\sim 1590\text{ cm}^{-1}$ can be regarded as the result of a slight frequency shift of the single Raman line found at $\sim 1575\text{ cm}^{-1}$ for single graphitic crystals that is ascribed to the bond stretching motion pairs of sp^2 C atoms present in olefinic chains or aromatic rings [29]. The ratios (I_D/I_G) of CNTs ($I_D/I_G = 0.23$) are much lower than that of pyrolyzed carbon ($I_D/I_G = 1.14$), indicating the higher degree of graphitization and larger graphite crystallites in CNTs than in pyrolyzed carbon [30]. Herein, after compositing with CNTs, the average ratio (I_D/I_G) of carbon/CNTs is much higher than that of the pyrolyzed carbon. A higher degree of graphitization of pyrolyzed carbon means higher electrical conductivity, which would also be demonstrated in electrochemical performance.

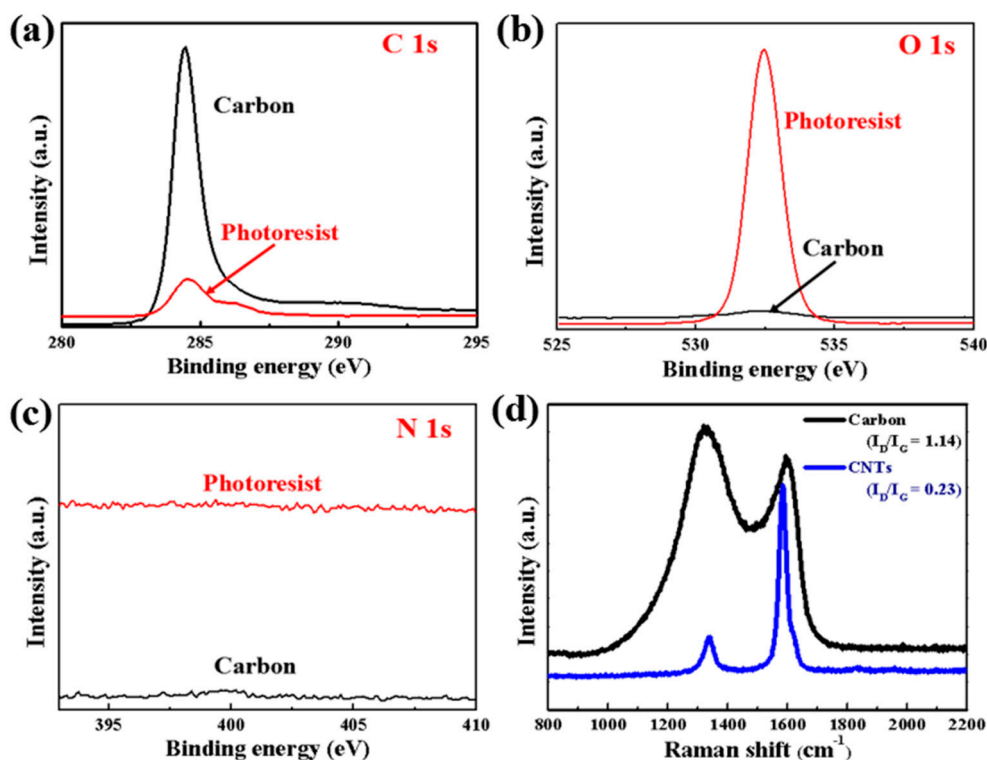


Figure 2. (a–c) XPS curves of GM-1060 photoresist and pyrolyzed carbon. (d) Raman spectra of pyrolyzed carbon and CNTs.

Figure 3a–c show SEM images of the surface of pyrolyzed carbon, and low-magnification and high-magnification SEM images of the carbon/CNT microelectrode surface. Different from the typical morphology of pyrolyzed carbon shown in Figure 3a, the CNT network is formed on the surface of

carbon/CNT microelectrodes, as shown in Figure 3b,c. Interestingly, during the development process, the CNTs firmly adsorbed on the surface of GM-1060. After pyrolysis, CNTs near the surface of pyrolyzed carbon were well bonded with the surface of carbon. Figure 3d shows an SEM image of a carbon/CNT microelectrode. The networking structure of carbon/CNTs will provide higher surface area than that of pyrolyzed carbon for energy storage. Figure 3e–g show the C/O/Si element distribution in the microelectrodes, which indicates that C is the main element in pyrolyzed carbon.

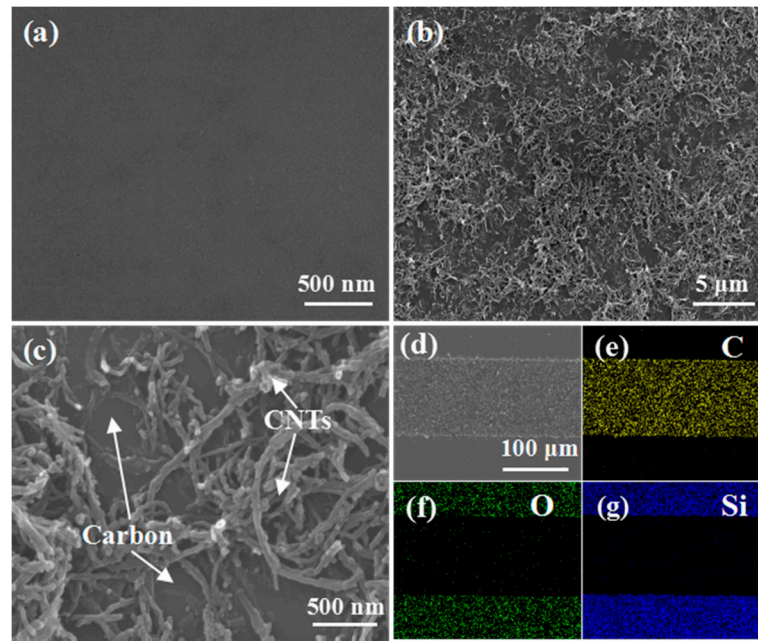


Figure 3. (a) SEM image of the surface of pyrolyzed carbon. (b) Low-magnification SEM image of carbon/CNT microelectrode surface. (c) High-magnification SEM image of carbon/CNT microelectrode surface. (d) SEM image of a carbon/CNT microelectrode. (e–g) Corresponding C/O/Si element mapping of carbon/CNTs microelectrode.

Figure 4 shows the electrochemical performances of the carbon-MSC and carbon/CNT-MSC. CV curves of carbon-MSC with rectangular-like shapes at low scan rates are shown in Figure 4a, indicating the typical EDLC behavior of carbon-MSC. However, as shown in Figure 4b, the CV curves of carbon/CNT-MSC are different, which indicates that the electrochemical behavior has changed due to CNT modification on the microelectrode surface. With the increase of scan rate, as shown in Figure 4c,d, the shapes of CV curves gradually transform into a fusiform for both carbon-MSC and carbon/CNT-MSC, which could be due to the polarization. The areal capacitance (C_{area}), stack capacitance (C_{stack}), energy density (E), and power density (P) are calculated based on Equations (1)–(4) [31]:

$$C_{\text{area}} = \frac{\int I(V)dV}{2As\Delta V} \quad (1)$$

$$C_{\text{stack}} = \frac{C_A}{d} \quad (2)$$

$$E = \frac{C_{\text{area}}\Delta V^2}{7200d} \quad (3)$$

$$P = \frac{E}{\Delta t} \times 3600 \quad (4)$$

where $\int I(V)dV$ is the integrated area of the CV curves and A is the area of the microelectrodes. s is the scan rate and ΔV is the potential window during CV tests. d is the thickness of microelectrodes and Δt is the discharge time.

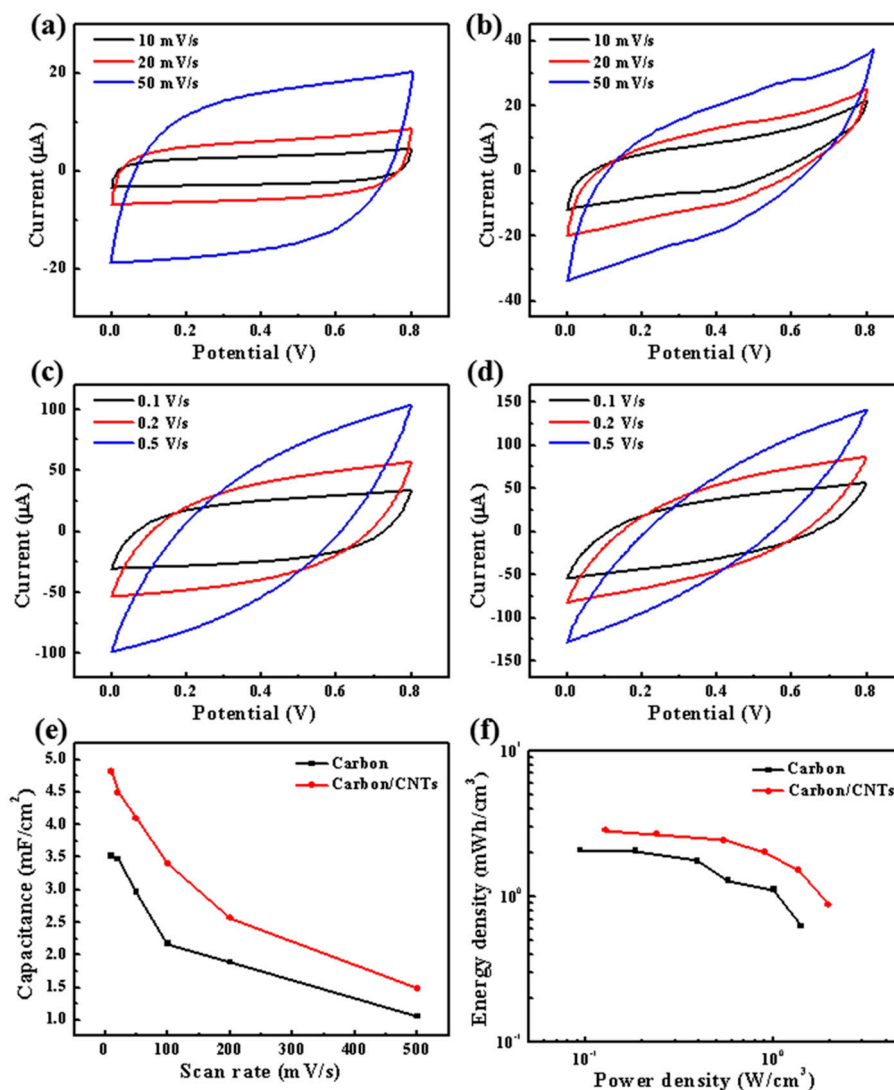


Figure 4. (a) CV curves of carbon-MSC at low scan rates. (b) CV curves of carbon/CNT-MSC at low scan rates. (c) CV curves of carbon-MSC at high scan rates. (d) CV curves of carbon/CNT-MSC at high scan rates. (e) Capacitance of carbon-MSC and carbon/CNT-MSC at different scan rates. (f) Energy density and power density of carbon-MSC and carbon/CNT-MSC, respectively.

The specific areal capacitance calculated from CV curves of carbon-MSC is 3.52 mF/cm^2 (23.4 F/cm^3) at the scan rate of 10 mV/s . Its maximum energy density is 2.08 mWh/cm^3 and maximum power density is 1.41 W/cm^3 . By contrast, the specific areal capacitance of carbon/CNT-MSC is 4.80 mF/cm^2 (32.0 F/cm^3) at the scan rate of 10 mV/s . In addition, its maximum energy density is 2.85 mWh/cm^3 , and maximum power density is 1.98 W/cm^3 . Based on the calculation, the relationship of capacitance of carbon-MSC and carbon/CNT-MSC at different scan rates, as well as energy density with power density of carbon-MSC and carbon/CNT-MSC, are presented in Figure 4e,f, respectively. It is obvious that the capacitance, energy density, and power density of carbon/CNT-MSC are higher than those of carbon-MSC. This result can be explained by the following two reasons: One is that the CNTs form a network structure on the surface of the microelectrodes which could increase the specific area of the microelectrodes, so that more ions can be absorbed and EDLC could be enhanced [32,33]. The other is that CNTs have higher electrical conductivity than pyrolyzed carbon, leading to faster charge transfer and higher response current during CV tests. Consequently, electrochemical performance can be improved by using this facile surface modification method for microelectrodes.

Galvanostatic charge-discharge (GCD) curves of carbon-MSC and carbon/CNT-MSC at a current density of 0.1 mA/cm^2 are demonstrated in Figure 5a,b. It is obvious that it takes more than 60 s for carbon/CNT-MSC to conduct charge/discharge process, much longer than that of carbon-MSC [34]. Also, the IR drop in GCD curves decreases. These differences indicate the improvement in both electrical conductivity and capacitance, and correspond to the explanation of capacitance increment in Figure 4. Figure 5c,d show the EIS curves of carbon-MSC and carbon/CNT-MSC with the frequency ranging from 0.01 to 100,000 Hz. EIS results indicate that the inner resistance of the microelectrode decreased because CNTs have higher conductivity than pyrolyzed carbon and the networking structure contributes to the fast charge transfer. Table 1 clearly exhibits the performance comparison of this work and other carbon-based MSCs [35–39]. The fabricated all-solid-state MSC (carbon/CNT-MSC) shows excellent electrochemical performance for energy storage.

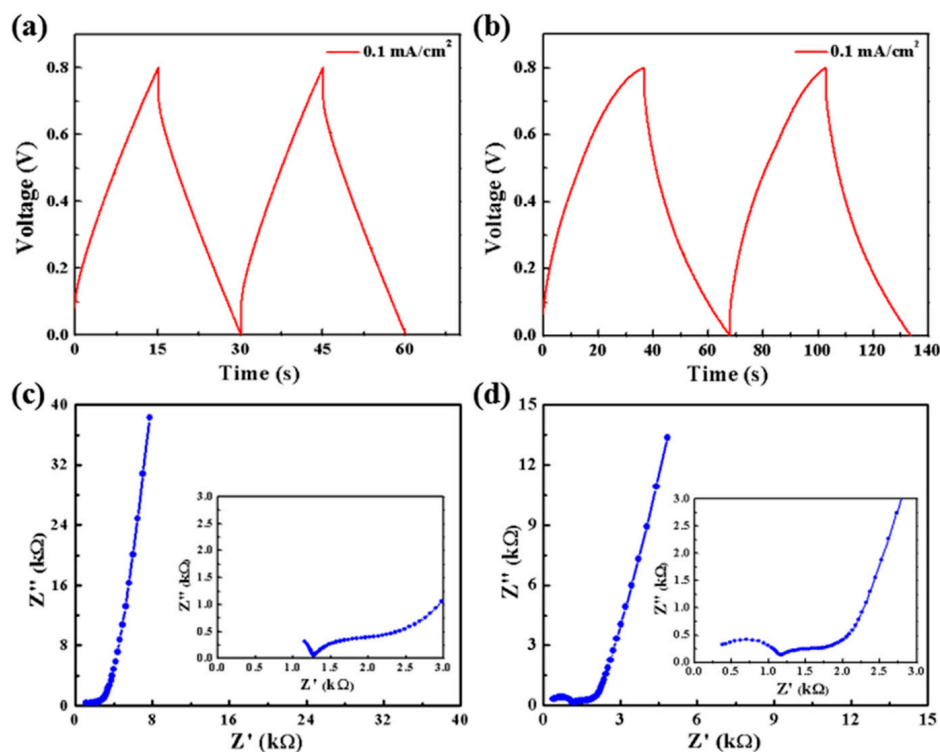


Figure 5. (a,b) GCD curves of carbon-MSC and carbon/CNT-MSC at a current density of 0.1 mA/cm^2 . (c,d) Electrochemical impedance spectroscopy (EIS) results of carbon-MSC and carbon/CNT-MSC with a frequency range from 0.01 to 100,000 Hz.

Table 1. Performance comparison of carbon-based MSCs.

Fabrication Method	Specific Capacitance (mF/cm^2)	Materials	Ref.
This work	4.80	Pyrolyzed carbon/CNTs	-
Mask-assisted filtration	9.8	Phosphorene/graphene	[35]
Lithography	5.9	Carbon	[36]
Preset filling	0.249	CNTs	[37]
Laser-assisted method	0.0627	Graphene	[38]
Nanoimprint lithography	0.008	Carbon	[39]

4. Conclusions

In this research, surface engineering of pyrolyzed carbon-based microelectrodes by microfabrication technology is proposed. It is found that the carbon/CNT-MSC shows higher electrochemical performance than the carbon-MSC. In addition, it is significant that our approach simplifies the microfabrication process of microelectrodes with surface modification by developing

photoresist in a mixture of developer and CNTs. This facile surface modification method for microelectrodes is a highly promising approach to obtain high-performance microelectrodes, showing great potential in applications of carbon-based microelectrodes.

Author Contributions: Conceptualization, B.X.; Methodology, T.H. and W.A.H.; Validation, Y.H. (Yue Huang), B.X. and X.H.; Formal Analysis, X.H.; Investigation, L.H. and M.T.; Data Curation, Y.H. (Yue Huang); Writing-Original Draft Preparation, L.H.; Writing-Review & Editing, T.H. and Y.H. (Yue Huang); Visualization, Y.H. (Yue Huang) and B.X.; Supervision, Y.H. (Yulai Han); Project Administration, L.H. and Y.H. (Yulai Han); Funding Acquisition, L.H. and Y.H. (Yulai Han).

Funding: This work was supported by the National Key Research and Development Program of China (2016YFA0202604), the National Natural Science Foundation of China (51579198), the Shenzhen Science and Technology Innovation Free Exploration Project (JCYJ20170818140127741), the Startup Foundation of Shenzhen Technology University (201701), and Wuhan Morning Light Plan of Youth Science and Technology (2017050304010316).

Conflicts of Interest: The authors declare no conflict of interest.

References

1. Simon, P.; Gogotsi, Y. Materials for electrochemical capacitors. *Nat. Mater.* **2008**, *7*, 845. [[CrossRef](#)] [[PubMed](#)]
2. Wang, K.; Zou, W.; Quan, B.; Yu, A.; Wu, H.; Jiang, P.; Wei, Z. An All-Solid-State Flexible Micro-supercapacitor on a Chip. *Adv. Energy Mater.* **2011**, *1*, 1068. [[CrossRef](#)]
3. Yang, P.; Mai, W. Flexible solid-state electrochemical supercapacitors. *Nano Energy* **2014**, *8*, 274. [[CrossRef](#)]
4. Yu, Z.; Tetard, L.; Zhai, L.; Thomas, J. Supercapacitor electrode materials: nanostructures from 0 to 3 dimensions. *Energy Environ. Sci.* **2015**, *8*, 702. [[CrossRef](#)]
5. Brousse, T.; Bélanger, D.; Long, J.W. To be or not to be pseudocapacitive? *J. Electrochem. Soc.* **2015**, *162*, A5185. [[CrossRef](#)]
6. Jiang, S.; Shi, T.; Zhan, X.; Xi, S.; Long, H.; Gong, B.; Li, J.; Cheng, S.; Huang, Y.; Tang, Z. Scalable fabrication of carbon-based MEMS/NEMS and their applications: a review. *J. Micromech. Microeng.* **2015**, *25*, 113001. [[CrossRef](#)]
7. Xiao, Y.; Huang, L.; Zhang, Q.; Xu, S.; Chen, Q.; Shi, W. Gravure printing of hybrid MoS₂@S-rGO interdigitated electrodes for flexible microsupercapacitors. *Appl. Phys. Lett.* **2015**, *107*, 013906. [[CrossRef](#)]
8. Beidaghi, M.; Gogotsi, Y. Capacitive energy storage in micro-scale devices: recent advances in design and fabrication of micro-supercapacitors. *Energy Environ. Sci.* **2014**, *7*, 867. [[CrossRef](#)]
9. Eustache, E.; Douard, C.; Retoux, R.; Lethien, C.; Brousse, T. MnO₂ thin films on 3D scaffold: microsupercapacitor electrodes competing with “bulk” carbon electrodes. *Adv. Energy Mater.* **2015**, *5*, 1500680. [[CrossRef](#)]
10. Hsia, B.; Kim, M.S.; Vincent, M.; Carraro, C.; Maboudian, R. Photoresist-derived porous carbon for on-chip micro-supercapacitors. *Carbon* **2013**, *57*, 395. [[CrossRef](#)]
11. Ranganathan, S.; McCreery, R.; Majji, S.M.; Madou, M. Photoresist-derived carbon for microelectromechanical systems and electrochemical applications. *J. Electrochem. Soc.* **2000**, *147*, 277. [[CrossRef](#)]
12. Wang, S.; Hsia, B.; Carraro, C.; Maboudian, R. High-performance all solid-state micro-supercapacitor based on patterned photoresist-derived porous carbon electrodes and an ionogel electrolyte. *J. Mater. Chem. A* **2014**, *2*, 7997. [[CrossRef](#)]
13. Jung, H.; Cheah, C.V.; Jeong, N.; Lee, J. Direct printing and reduction of graphite oxide for flexible supercapacitors. *Appl. Phys. Lett.* **2014**, *105*, 053902. [[CrossRef](#)]
14. Beidaghi, M.; Wang, C. Supercapacitors: Micro-Supercapacitors Based on Interdigital Electrodes of Reduced Graphene Oxide and Carbon Nanotube Composites with Ultrahigh Power Handling Performance. *Adv. Funct. Mater.* **2012**, *22*, 4500. [[CrossRef](#)]
15. Gao, W.; Singh, N.; Song, L.; Liu, Z.; Reddy, A.L.M.; Ci, L.; Vajtai, R.; Zhang, Q.; Wei, B.; Ajayan, P.M. Direct laser writing of micro-supercapacitors on hydrated graphite oxide films. *Nat. Nano* **2011**, *6*, 496. [[CrossRef](#)] [[PubMed](#)]
16. Sun, L.; Wang, X.; Zhang, K.; Zou, J.; Zhang, Q. Metal-free SWNT/carbon/MnO₂ hybrid electrode for high performance coplanar micro-supercapacitors. *Nano Energy* **2016**, *22*, 11. [[CrossRef](#)]

17. Hu, H.; Pei, Z.; Ye, C. Recent advances in designing and fabrication of planar micro-supercapacitors for on-chip energy storage. *Energy Storage Mater.* **2015**, *1*, 82. [[CrossRef](#)]
18. Wu, B.; Kumar, A. Extreme ultraviolet lithography and three dimensional integrated circuit—A review. *Appl. Phys. Rev.* **2014**, *1*, 011104. [[CrossRef](#)]
19. Kwon, S.; Jung, D.; Lim, H.; Kim, G.; Choi, K.B.; Lee, J. Laser-assisted selective lithography of reduced graphene oxide for fabrication of graphene-based out-of-plane tandem microsupercapacitors with large capacitance. *Appl. Phys. Lett.* **2017**, *111*, 143903. [[CrossRef](#)]
20. Zhou, P.; Yang, X.; He, L.; Hao, Z.; Luo, W.; Xiong, B.; Xu, X.; Niu, C.; Yan, M.; Mai, L. The Young's modulus of high-aspect-ratio carbon/carbon nanotube composite microcantilevers by experimental and modeling validation. *Appl. Phys. Lett.* **2015**, *106*, 111908. [[CrossRef](#)]
21. An, Z.; He, L.; Toda, M.; Yamamoto, G.; Hashida, T.; Ono, T. Microstructuring of carbon nanotubes-nickel nanocomposite. *Nanotechnology* **2015**, *26*, 195601. [[CrossRef](#)]
22. He, L.; Toda, M.; Kawai, Y.; Miyashita, H.; Omori, M.; Hashida, T.; Berger, R.; Ono, T. Fabrication of CNT-carbon composite microstructures using Si micromolding and pyrolysis. *Microsyst. Technol.* **2014**, *20*, 201. [[CrossRef](#)]
23. Hong, X.; He, L.; Ma, X.; Yang, W.; Chen, Y.; Zhang, L.; Yan, H.; Li, Z.; Mai, L. Microstructuring of carbon/tin quantum dots via a novel photolithography and pyrolysis-reduction process. *Nano Res.* **2017**, *10*, 3743. [[CrossRef](#)]
24. Kim, M.S.; Hsia, B.; Carraro, C.; Maboudian, R. Flexible micro-supercapacitors with high energy density from simple transfer of photoresist-derived porous carbon electrodes. *Carbon* **2014**, *74*, 163. [[CrossRef](#)]
25. Yang, W.; He, L.; Tian, X.; Yan, M.; Yuan, H.; Liao, X.; Meng, J.; Hao, Z.; Mai, L. Carbon-MEMS-Based Alternating Stacked MoS₂@ rGO-CNT Micro-Supercapacitor with High Capacitance and Energy Density. *Small* **2017**, *13*, 1700639. [[CrossRef](#)]
26. Yang, Y.; He, L.; Tang, C.; Hu, P.; Hong, X.; Yan, M.; Dong, Y.; Tian, X.; Wei, Q.; Mai, L. Improved conductivity and capacitance of interdigital carbon microelectrodes through integration with carbon nanotubes for micro-supercapacitors. *Nano Res.* **2016**, *9*, 2510. [[CrossRef](#)]
27. Yin, C.; He, L.; Wang, Y.; Liu, Z.; Zhang, G.; Zhao, K.; Tang, C.; Yan, M.; Han, Y.; Mai, L. Pyrolyzed carbon with embedded NiO/Ni nanospheres for applications in microelectrodes. *RSC Adv.* **2016**, *6*, 43436. [[CrossRef](#)]
28. Ma, X.; Feng, S.; He, L.; Yan, M.; Tian, X.; Li, Y.; Tang, C.; Hong, X.; Mai, L. Rapid, all dry microfabrication of three-dimensional Co₃O₄/Pt nanonetworks for high-performance microsupercapacitors. *Nanoscale* **2017**, *9*, 11765. [[CrossRef](#)] [[PubMed](#)]
29. Zhao, Y.; Chen, G.; Du, Y.; Xu, J.; Wu, S.; Qu, Y.; Zhu, Y. Plasmonic-enhanced Raman scattering of graphene on growth substrates and its application in SERS. *Nanoscale* **2014**, *6*, 13754. [[CrossRef](#)]
30. Wang, H.; Peng, C.; Zheng, J.; Peng, F.; Yu, H. Design, synthesis and the electrochemical performance of MnO₂/C@ CNT as supercapacitor material. *Mater. Res. Bull.* **2013**, *48*, 3389. [[CrossRef](#)]
31. Zhang, Y.; Wang, Y.; Cheng, T.; Lai, W.; Pang, H.; Huang, W. Flexible supercapacitors based on paper substrates: a new paradigm for low-cost energy storage. *Chem. Soc. Rev.* **2015**, *44*, 5181. [[CrossRef](#)]
32. Park, B.Y.; Taherabadi, L.; Wang, C.; Zoval, J.; Madou, M.J. Electrical properties and shrinkage of carbonized photoresist films and the implications for carbon microelectromechanical systems devices in conductive media. *J. Electrochem. Soc.* **2005**, *152*, J136. [[CrossRef](#)]
33. Xu, G.; Zheng, C.; Zhang, Q.; Huang, J.; Zhao, M.; Nie, J.; Wang, X.; Wei, F. Binder-free activated carbon/carbon nanotube paper electrodes for use in supercapacitors. *Nano Res.* **2011**, *4*, 870. [[CrossRef](#)]
34. Yun, J.; Kim, D.; Lee, G.; Ha, J.S. All-solid-state flexible micro-supercapacitor arrays with patterned graphene/MWNT electrodes. *Carbon* **2014**, *79*, 156. [[CrossRef](#)]
35. Xiao, H.; Wu, Z.S.; Chen, L.; Zhou, F.; Zheng, S.; Ren, W.; Cheng, H.M.; Bao, X. One-step device fabrication of phosphorene and graphene interdigital micro-supercapacitors with high energy density. *ACS Nano* **2017**, *11*, 7284. [[CrossRef](#)] [[PubMed](#)]
36. Pal, R.K.; Kundu, S.C.; Yadavalli, V.K. Fabrication of Flexible, Fully Organic, Degradable Energy Storage Devices Using Silk Proteins. *ACS Appl. Mater. Interfaces* **2018**, *10*, 9620. [[CrossRef](#)] [[PubMed](#)]
37. Song, Y.; Chen, H.; Chen, X.; Wu, H.; Guo, H.; Cheng, X.; Meng, B.; Zhang, H. All-in-one piezoresistive-sensing patch integrated with micro-supercapacitor. *Nano Energy* **2018**, *53*, 189. [[CrossRef](#)]

38. Ye, J.; Tan, H.; Wu, S.; Ni, K.; Pan, F.; Liu, J.; Tao, Z.; Qu, Y.; Ji, H.; Simon, P.; Zhu, Y. Direct Laser Writing of Graphene Made from Chemical Vapor Deposition for Flexible, Integratable Micro-Supercapacitors with Ultrahigh Power Output. *Adv. Mater.* **2018**, *30*, e1801384. [[CrossRef](#)] [[PubMed](#)]
39. Lochmann, S.; Grothe, J.; Eckhardt, K.; Leistenschneider, D.; Borchardt, L.; Kaskel, S. Nanoimprint lithography of nanoporous carbon materials for micro-supercapacitor architectures. *Nanoscale* **2018**, *10*, 10109. [[CrossRef](#)] [[PubMed](#)]



© 2019 by the authors. Licensee MDPI, Basel, Switzerland. This article is an open access article distributed under the terms and conditions of the Creative Commons Attribution (CC BY) license (<http://creativecommons.org/licenses/by/4.0/>).